

Hydrogen bonding lights up overtones in pyrazoles

T. N. Wassermann, C. A. Rice, and M. A. Suhm^{a),b)}

Institut für Physikalische Chemie, Universität Göttingen, Tammannstrasse 6, 37077 Göttingen, Germany

D. Luckhaus^{a),c)}

Chemistry Department, University of British Columbia, 6174 University Blvd., Vancouver, British Columbia V6T 1Z3, Canada

(Received 16 August 2007; accepted 15 October 2007; published online 18 December 2007)

The spectral complexity in the NH stretching mode of hydrogen-bonded pyrazoles is traced back to an extensive Fermi resonance system involving combinations and overtones of at least four aromatic ring modes with significant in plane hydride bending character. The couplings are shown to be inherent in the monomer, but hydrogen bonding is required to bring them into resonance with the NH stretching chromophore. A cost-efficient variational “monomers-in-clusters” model is presented and applied to a five-dimensional subspace of pyrazole. Spectra of substituted pyrazoles confirm the robustness of the coupling, which remains dark in strained dimers, but lights up in linearly hydrogen-bonded trimers. © 2007 American Institute of Physics. [DOI: 10.1063/1.2806181]

INTRODUCTION

Since the first description of a resonance between the symmetric stretching fundamental and the bending overtone in CO₂ by Fermi in 1931,¹ such Fermi resonances between two vibrations with $\approx 1:2$ frequency ratio have been among the best studied pathways for intramolecular vibrational relaxation processes. With increasing molecular size and density of states, they become more frequent, although strong resonances usually require a close vicinity of the active atoms. Few Fermi resonances are as basic and well developed as the one in CO₂. Often, they have to be “tuned in” by reshaping or climbing the potential energy hypersurface. The latter is the case for the resonance between CH stretching and bending modes, which can be tuned in by moving to anharmonically distorted higher CH stretching excitations.^{2,3}

The former approach of reshaping the potential energy hypersurface is possible via intermolecular interactions. Hydrogen bond-induced redshifts can change hydride stretching fundamentals quite significantly. They may thus come into resonance with overtones or combination levels of lower frequency skeletal vibrations of the same molecule, which are typically less sensitive to hydrogen bonding. This phenomenon has been investigated in detail for carboxylic acids (see, e.g., Refs. 4–6), where Fermi resonances shape the coarse-grained structure of the OH stretching band in the hydrogen bonded dimers, whereas they are not active in the corresponding monomers. Recently, a similar effect has been found for the NH stretching band of the hydrogen bonded 7-azaindole dimer and has been addressed in an experimental⁷ and a comprehensive theoretical study.⁸

In both azaindole and carboxylic acids, the hydrogen bond donor and acceptor sites are separated by three chemical bonds (H—X—C=X) with bond angles close to 120°.

This geometry leads to symmetric, strain-free doubly hydrogen bonded dimers. The switch from local monomer X—H stretching dynamics to strongly coupled dimer dynamics is thus discontinuous or sudden.

It would be desirable to follow the onset of Fermi resonances in a more continuous way, by gradually intensifying its cause, the intermolecular perturbation. A first step in this direction would be to arrange the hydrogen bonding functionality in a pattern which is less suitable for dimerization, keeping in mind the directionality of hydrogen bonds. This is the case for pyrazoles, where the donor and acceptor sites are separated by only two chemical bonds (H—N—N) at an $\approx 120^\circ$ angle. A symmetric dimer formed between two pyrazoles will necessarily have bent hydrogen bonds, whereas trimers can accommodate more or less linear hydrogen bond structures. This is illustrated in Fig. 1. As a consequence, planar C_{3h} pyrazole trimers or winding chains are often observed in the crystalline solids,^{9–11} unless sterical constraints induced by bulky ring substitution enforce C_{2h} dimer or strongly folded tetramer formation. Concerted and stepwise proton tunneling in cyclic pyrazole oligomers is a very sensitive probe of this subtle interplay between cooperative bonding, hydrogen bond strain, and sterical hindrance.^{12–16}

In solution and in the gas phase, cyclic clusters beyond the dimer usually prevail as well.^{17,18} Under most conditions the cyclic C_{2h} dimer of pyrazole, postulated by W. Hückel *et al.* in 1940,¹⁹ only represents a minor component.²⁰ It is best prepared either at high temperatures,¹⁸ where the strong temperature dependence renders the determination of the band center difficult, or in supersonic jet expansions.²¹ The latter method has provided an accurate band center for the IR-active dimer stretching fundamental at 3255 cm⁻¹ for the first time. In contrast to the case of carboxylic acid dimers, which feature similar strength hydrogen bonds, pyrazole dimer shows a simple and narrow IR-active NH transition with no evidence for pronounced vibrational coupling.²¹

Spectra reminiscent of the carboxylic acid dimer case

^{a)}Authors to whom correspondence should be addressed.

^{b)}Electronic mail: msuhm@gwdg.de

^{c)}Electronic mail: dluckhaus@chem.ubc.ca

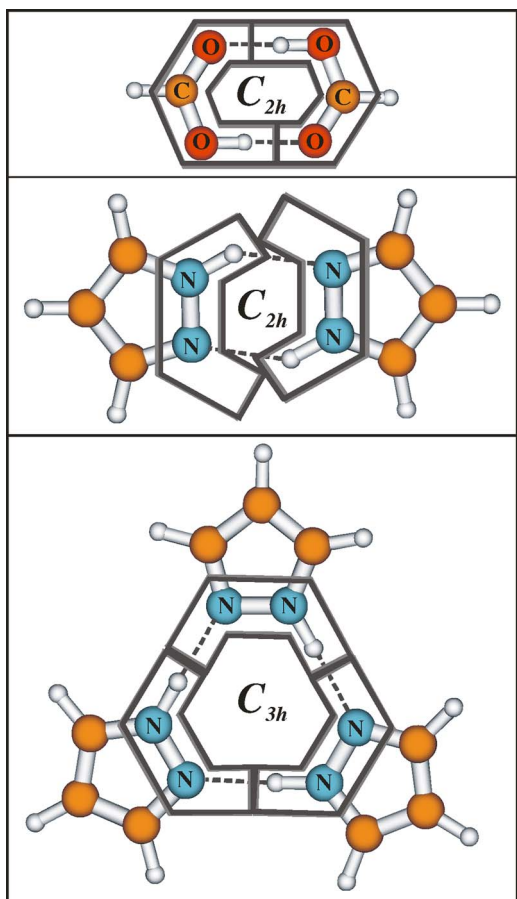


FIG. 1. (Color online) Illustration of the hydrogen bond geometry in carboxylic acid dimers and pyrazole dimers and trimers. Pyrazole dimers do not correspond to a strain-free arrangement.

have been observed in cyclic oligomers of substituted pyrazoles.^{18,22–25} In all cases, a broad, often structured band dominates the NH stretching spectrum. Indeed, the spectra obtained in seeded supersonic jet expansions of the parent species reveal that the breadth of the higher cluster band is neither due to thermal broadening effects nor to cluster isomerism.²¹

The onset of spectral complexity in pyrazole whenever the NH stretching fundamental falls in the 2500–3200 cm^{-1} range has been put in the context of Fermi resonance interactions by several authors.^{18,22–25} We summarize a few of these observations.

- (i) In 1967 Zecchina *et al.* assigned four ring stretching vibrations of the parent pyrazole in the range of 1350–1530 cm^{-1} and explained the broad NH stretching band near 2500–3000 cm^{-1} by Fermi couplings with these lower frequency vibrations.²²
- (ii) In 1976 Wolff and Müller discussed Fermi resonances in the aggregates of pyrazole between the NH stretching vibration and lower frequency modes involving ring vibrations and NH deformation modes. They observed similar band structures for self-associated species as well as for mixed aggregates with hydrogen bond acceptors.²³
- (iii) In 1979 Tabacik *et al.* found somewhat less pronounced Fermi resonances in monomeric

N-deuteropyrazoles between the ND oscillator and low frequency ring vibrations.²⁴ Isotope substitution indeed represents a third way of tuning two vibrations into resonance, along with the overtone tuning³ and intermolecular interaction strategies⁴ outlined above.

- (iv) In 2000 Orza *et al.* reported Fermi resonances in complexes formed by methylated NH and ND pyrazoles. The same phenomenon occurred in aqueous solution with water mimicking the surrounding in the self-aggregates.²⁵ They argued that the essential ingredient for the spectral features is the change in electronic structure induced by hydrogen bonding.

What is still missing is a combined experimental and theoretical mapping of these phenomena as a function of NH stretching frequency or cluster size. In the present work, we will outline the buildup of intramolecular Fermi resonances as the NH stretching force constant is reduced, thus explaining the coarse-grained vibrational structure in the region between 2800 and 3200 cm^{-1} without having to invoke any other electronic structure change. The extension of the multidimensional anharmonic “monomers-in-dimers” model, successfully applied to carboxylic dimers,⁴ to a “monomers-in-clusters” (MIC) model allows the identification of the key vibrations that contribute to the complex band pattern. Experimental spectra and harmonic force field calculations for pyrazoles with CH_3 or CF_3 substituents on the ring support the results.

EXPERIMENTAL

Supersonic jet IR spectra of the NH stretching vibrations of pyrazole derivatives seeded in He were recorded using the ragout jet Fourier transform infrared (FTIR) technique,²⁶ a pneumatically pulsed room temperature slit jet expansion probed by a synchronized 2 cm^{-1} resolution FTIR scan. The spectra of the parent compound were presented before.²¹ By using a relatively wide slit (0.5 mm), there are sufficient collisions in the expansion to promote the formation of dimers, trimers, and possibly also some larger clusters of the heterocyclic compounds despite their low vapor pressure. Only for 3,5-dimethylpyrazole (99%, Alfa Aesar), a heatable nozzle experiment²⁷ (nozzle temperature ≈ 100 °C, sample temperature ≈ 80 °C, 10×0.5 mm² slit nozzle) was required to generate a sufficient density of dimers and larger clusters. In the room temperature experiments, the expansion can be sustained for 140 ms despite a slit length of 120 mm, because the gas is diluted in a 23 m³ buffer chamber, before being pumped away by a series of Roots blowers at 2000 m³ h⁻¹. After a recovery period of up to 60 s, the process is repeated and the resulting spectra are coadded. The Bruker IFS 66v/S FTIR spectrometer is equipped with a Globar light source, a CaF_2 beamsplitter and an optical filter (2.8–5.0 μm). After crossing the expansion zone, the collimated IR beam is focused by a parabolic mirror ($f=43$ mm) onto a large area InSb detector, which is located in an externally evacuated detector chamber.

The pyrazole gas mixtures are prepared by flowing He ($\geq 99.996\%$, Air Liquide) at 1.2–1.8 bar through a glass saturator containing the solid pyrazoles [3(5)-methyl-

pyrazole: 97%, Fluka; 4-methylpyrazole: 99%, Aldrich; 3(5)-(trifluoromethyl)pyrazole: 99%, Aldrich; and 3,5-bis(trifluoromethyl)pyrazole: 97%, Fluorochem] at 293–298 K. The stagnation pressure in the reservoir ranges from 1.0 to 1.5 bar.

THEORETICAL

The electronic structure, potential scans, and harmonic frequency calculations described in this work were performed using GAUSSIAN 03 (Ref. 28) either at the B3LYP level and a 6–31+G* basis set (in the following referred to as “B3LYP calculations”) or with the *ab initio* MP2 perturbation approach using the 6–311+G** basis set (“MP2 calculations” in the following). For the parent pyrazole, anharmonic frequency calculations based on perturbation theory²⁹ were also performed in order to explore the anharmonicity of the N–H stretching vibration in a simple way.

The multidimensional anharmonic model calculations described here (MIC) build on the monomers-in-dimers model outlined in Ref. 4. This model starts with the monomer and modifies its vibrational wavenumbers according to the influence of hydrogen bonding, leaving the nature of the vibrational coordinates and the couplings unchanged.

The main parameter is the softening of the NH oscillator caused by the hydrogen bond formation. The weakening of the NH bond shifts its stretching frequency into a region of other intramolecular vibrational energy levels. Following local NH stretch excitation, the intrinsic coupling with these degrees of freedom is activated by the resonance condition and leads to the distribution of vibrational energy over all involved levels.

The shift in the model calculations is introduced by a simple scaling procedure.^{30,31} The monomer vibrational Hamiltonian neglecting vibrational angular momentum terms in reduced normal coordinate representation q_k with conjugate momenta \hat{p}_k is given as^{32,33}

$$\hat{H}/hc = \left[\sum_{k=1}^{21} \frac{\omega_k}{2} (\hat{p}_k^2 + q_k^2) \right] + V_{\text{anharm}}(q_1, \dots, q_{21}), \quad (1)$$

where

$$\hat{p}_k = -i \frac{\partial}{\partial q_k} \quad (2)$$

and

$$q_k = 2\pi Q_k \sqrt{\frac{\omega_k c}{h}}. \quad (3)$$

h is Planck's constant, c the speed of light, $i = \sqrt{-1}$, and Q_k are the usual mass-weighted normal coordinates with corresponding harmonic wavenumbers ω_k . V_{anharm} collects all anharmonic contributions to the potential energy.

Within the harmonic approximation (i.e., $V_{\text{anharm}}=0$) a change of the fundamental transition wavenumber from the monomer (ω_{monomer}) to a complex (ω_{complex}) can be described exactly by scaling the monomer wavenumbers ω_k in [Eq. (3)].

$$\omega_k^{\text{sc}} = f_k \omega_k = \frac{\omega_{k,\text{complex}}}{\omega_{k,\text{monomer}}} \omega_k. \quad (4)$$

Different sources can be used for ω_{monomer} and ω_{complex} to obtain the scaling factor f_k , such as theoretical predictions or experimental fundamental wavenumbers. In order to retain the functional form of the potential in terms of reduced coordinates (q_k), the scaling has to be effected according to the following equations, which define the effective MIC Hamiltonian:

$$\hat{H}/hc = \sum_{k=1}^{21} \frac{\omega_k}{2} (f_k^2 \hat{p}_k^2 + q_k^2) + V_{\text{anharm}}(q_1, \dots, q_{21}). \quad (5)$$

Note that the potential function has exactly the same form as in Eq. (1), but with the reduced coordinates redefined in terms of mass-weighted normal coordinates,

$$q_k = 2\pi Q_k \sqrt{\frac{\omega_k^{\text{sc}} c}{h}}. \quad (6)$$

As has already been emphasized in Ref. 4, this model cannot account for the experimentally observed fine structure that corresponds to energy flow on longer (\geq picoseconds) timescales nor does the model describe the increase in NH oscillator strength upon complexation. Nevertheless, the relative intensities within the NH band system should be reasonably well described, as they mainly depend on the degree of the coupling. Thus, the MIC approach constitutes an effective method to identify the main contributions to the coarse-grained vibrational structure and to model the dominant energy flow paths.

The first step in these calculations is a search for coupling partners in the relevant spectral range. For this purpose, a systematic search for harmonic a' combination states involving up to four quanta in arbitrary normal modes of C_s -symmetric pyrazole was performed. For the promising combinations, preliminary scans in two or three dimensions were carried out in order to find strong coupling partners. These calculations were performed with the B3LYP functional and a 6–31+G* basis set using GAUSSIAN 03.²⁸

Pyrazole possesses four ring stretching vibrations²² in the harmonic frequency range between 1300 and 1600 cm^{-1} with strong δ_{NH} character, which is expected to promote the coupling. As these modes also have significant CH bend character (δ_{CH}), we simply label them ω_{1-4} , in accordance with Ref. 22. A five-dimensional (5D) calculation was carried out including the NH stretching vibration ν_{NH} and these four vibrations ω_{1-4} . More than 5.2×10^4 points were calculated on the five-dimensional B3LYP/6–31+G* potential energy (PES) and dipole hypersurface along the normal coordinates of the corresponding vibrations in the range from –6.0 to +6.0. A refinement of the surface was carried out using the technique of successive averaged spline interpolations,^{32,33} resulting in a smoother hypersurface on equidistant grids with a step width of 0.5 in each coordinate. A second spline-interpolated hypersurface based on $\approx 10.2 \times 10^4$ points was evaluated at the *ab initio* MP2 level using the 6–311+G** basis set in order to test the sensitivity of

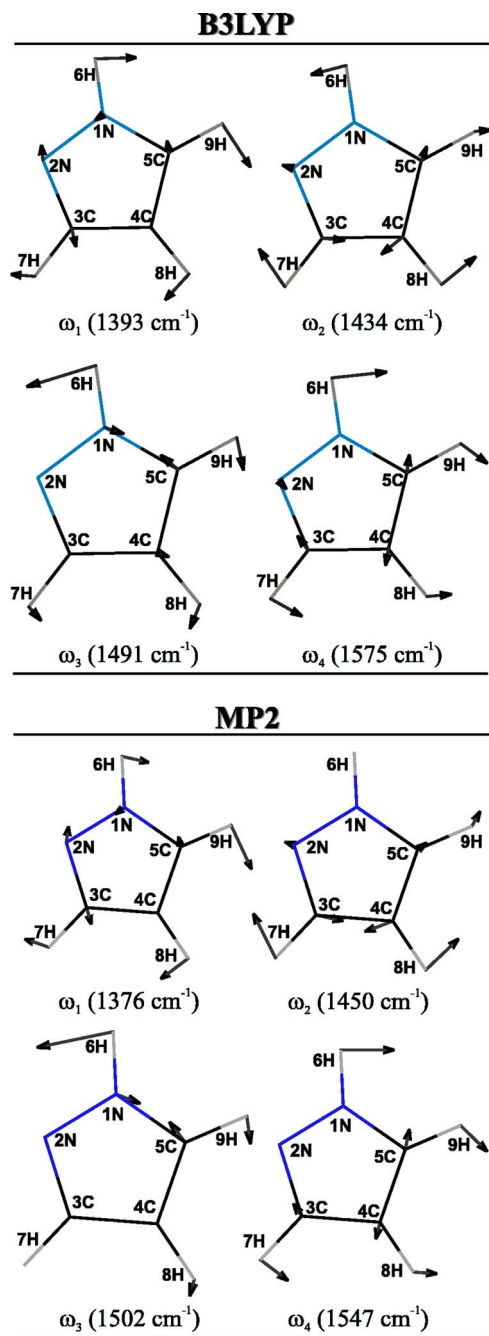


FIG. 2. (Color online) Approximate normal coordinate motions of the four ring stretching vibrations ω_{1-4} and harmonic wavenumbers as calculated at B3LYP/6-31+G* and MP2/6-311+G** level (see also Table V).

the MIC model with respect to differences in the electronic structure approach. The vibrational problem was solved employing a successive adiabatic truncation in a discrete variable representation.³⁴ The contributing vibrations to the MIC energy levels were identified by the overlap with harmonic vibrational wavefunctions.

RESULTS AND DISCUSSION

MIC calculations for pyrazole

Figure 2 shows the normal modes that have been found to be the main coupling partners of the NH stretching vibration (the in plane ring deformations ω_{1-4}), including their

TABLE I. Scaling factors f_{NH} applied to ω_{NH} in the MIC calculations according to Eq. (4). Target frequencies used for the calculations were taken from Ref. 21.

f_{NH}	Source ^a	Target ^b	Trace ^c
1	...	<i>M</i>	(b)
0.940	B3LYP/6-31+G*	<i>D</i>	(c)
0.920	MP2/aug-cc-pVDZ	<i>D</i>	(d)
0.906	...	<i>D</i>	(e)
0.890	B3LYP/6-31+G*	<i>T</i>	(f)
0.864	B3LYP/aug-cc-pVDZ	<i>T</i>	(g)
0.825	Expt.	<i>T</i>	(h)
0.810	Expt.	<i>T</i>	(i)

^aSource which suggests a particular scaling factor.

^bTargeted pyrazole species. *M*=monomer, *D*=dimer, *T*=trimer, and higher clusters.

^cTrace of the calculated MIC spectra in Figs. 3 and 4.

harmonic wavenumbers, as calculated at the B3LYP/6-31+G* and MP2/6-311+G** levels (see also Table V). As expected they coincide with the modes with the most pronounced NH-bend character.

The adjustable parameter in the multidimensional anharmonic calculations is the scaling factor f_{NH} which is applied to the NH stretching mode prior to the variational solution of the vibrational problem. The ring vibrations are left unchanged in most calculations, because they are affected only slightly by hydrogen bonding. Several scaling factors (Table I) were applied to the NH stretching vibration to either reproduce quantum chemical predictions or experimental values for various cluster sizes.²¹ Intermediate scaling factors were added in order to follow the smooth evolution of the spectra from the monomer to the higher cluster. Different sources of reference wavenumbers ω_{monomer} and ω_{complex} [see Eq. (4)] were used in the scaling resulting in a range of ω_k^{sc} values.

The spectral appearance changes profoundly with decreasing scaling factor as can be seen in Fig. 3. In these calculations the ring stretching vibrations ω_{1-4} remain unscaled. The scaling of ω_{1-4} based on calculated harmonic wavenumbers in the trimer shifts the entire band system toward higher wavenumbers (by ≈ 30 – 100 cm^{-1}), without changing its general appearance.

The NH stretching vibration is seen to walk into resonance once the scaling factor f_{NH} falls below ≈ 0.890 [trace (f)]. The ring vibration overtones and combination bands—originally dark states—start to light up according to their acquired NH stretching character. Beyond $f_{\text{NH}} \approx 0.810$, the NH vibration walks out of the zone of resonance.

The NH stretching character ($\% \nu_{\text{NH}}$) in the strongly coupled MIC spectra [e.g., Fig. 3(h)] is smeared out over a large number of different energy levels. As can be seen from Table II, none of the transitions corresponds predominantly to a ν_{NH} transition but many of them show strong mixing with the NH mode so that the character of the excited NH stretch is redistributed over several vibrational levels leading to this strong resonance phenomenon.

Figure 4 shows simulated spectra based on the MP2 PES, obtained by applying the same scaling factors to the NH stretching vibration as for Fig. 3 (f_{NH} in Table I). The

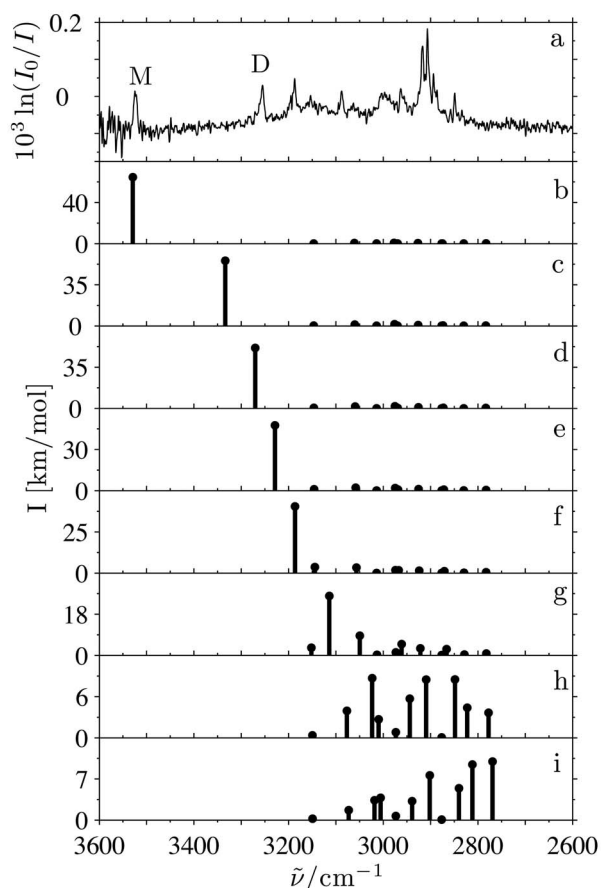


FIG. 3. MIC stick spectra based on B3LYP PES with different scaling factors compared to the experimental spectrum from Ref. 21. (a) Experimental spectrum. *M* and *D* mark the position of the monomer and dimer absorption bands, respectively. [(b)–(i)] Theoretical spectra obtained in MIC calculations with increasing redshift of the NH stretching vibration. For the different f_{NH} corresponding to Eq. (4) see Table I.

main contributions to the resulting vibrational states of one exemplary spectrum [Fig. 4(h)] are summarized in Table III (to be compared with Table II).

A first assessment of the two five-dimensional treatments refers to the predicted position of the unperturbed monomer NH stretching fundamental (Figs. 3 and 4, trace (b), scaling

TABLE II. Main contributions to the MIC wavefunctions in Fig. 3(h) (B3LYP PES). Only the major two to three harmonic components (see Fig. 2) are listed (in parentheses: contributions in percent).

$\tilde{\nu}_{\text{MIC}}$ (cm ⁻¹)	Contributing vibrations	
2777	$2\omega_1$ (76)	ν_{NH} (9), $2\omega_2$ (6)
2823	$\omega_1 + \omega_2$ (54)	$2\omega_1$ (15), ν_{NH} (13)
2848	$\omega_1 + \omega_2$ (39)	$2\omega_2$ (24), ν_{NH} (18)
2877	$\omega_1 + \omega_3$ (92)	$2\omega_2$ (3)
2909	$2\omega_2$ (52)	$\omega_2 + \omega_3$ (20), ν_{NH} (13)
2944	$\omega_2 + \omega_3$ (68)	ν_{NH} (11)
2973	$\omega_1 + \omega_4$ (59)	$2\omega_3$ (35)
3010	$\omega_2 + \omega_4$ (44)	$2\omega_3$ (22), $\omega_1 + \omega_4$ (21)
3024	$\omega_2 + \omega_4$ (51)	$2\omega_3$ (21), ν_{NH} (13)
3077	$\omega_3 + \omega_4$ (88)	ν_{NH} (9)
3150	$2\omega_4$ (95)	$\omega_3 + \omega_4$ (1)

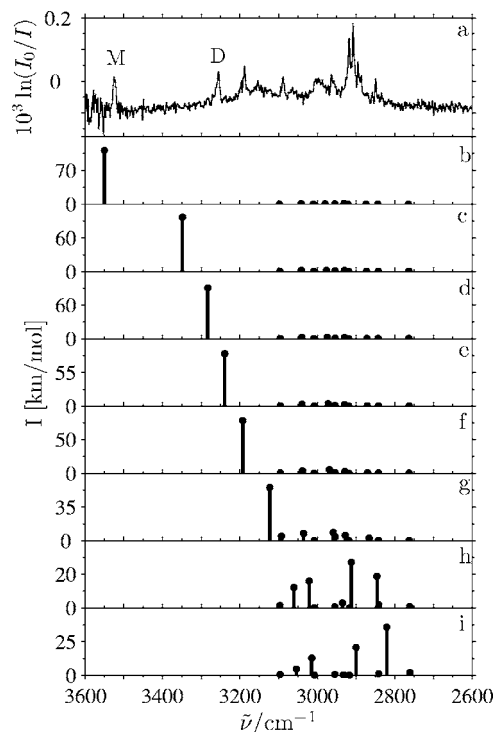


FIG. 4. MIC stick spectra based on MP2 PES with different scaling factors compared to the experimental spectrum from Ref. 21. (a) Experimental spectrum. *M* and *D* mark the position of the monomer and dimer absorption bands, respectively. [(b)–(i)] Theoretical spectra obtained in MIC calculations with increasing redshift of the NH stretching vibration. For the different f_{NH} corresponding to Eq. (4) see Table I.

factor $f_{\text{NH}}=1$). The B3LYP based prediction (3529 cm^{-1}) falls quite close to the experimental band position of 3523 cm^{-1} .^{20,21} The MP2 prediction amounts to 3550 cm^{-1} , still in good agreement with the experimental position.

In line with a slightly softer B3LYP NH oscillator, the scaling factor required to reproduce the experimental dimer absorption is closer to 1 [$f_{\text{NH}} \approx 0.920$, see also Fig. 3(d), where $\nu_{\text{NH}}=3271\text{ cm}^{-1}$] than in the MP2 case [$f_{\text{NH}} \approx 0.906$, see also Fig. 4(e), where $\nu_{\text{NH}}=3239\text{ cm}^{-1}$]. Possibly, the MP2 hypersurface would profit from the inclusion of further degrees of freedom.

Comparison of the approximate normal coordinate dis-

TABLE III. Main contributions to the MIC wavefunctions in Fig. 4(h) (MP2 PES). Only the major one to three harmonic components (see Fig. 2) are listed (in parentheses: contributions in percent).

$\tilde{\nu}_{\text{MIC}}$ (cm ⁻¹)	Contributing vibrations	
2762	$2\omega_1$ (96)	ν_{NH} (1), $\omega_1 + \omega_3$ (1)
2841	$\omega_1 + \omega_2$ (86)	$\omega_1 + \omega_3$ (6), ν_{NH} (4)
2846	$\omega_1 + \omega_3$ (40)	ν_{NH} (28), $\omega_1 + \omega_2$ (12)
2912	$\omega_1 + \omega_3$ (51)	ν_{NH} (23), $2\omega_3$ (9)
2917	$\omega_1 + \omega_4$ (96)	
2935	$2\omega_2$ (82)	ν_{NH} (7), $2\omega_3$ (7)
2955	$\omega_2 + \omega_3$ (94)	$\omega_2 + \omega_4$ (4)
3008	$\omega_2 + \omega_4$ (93)	$\omega_2 + \omega_3$ (4)
3021	$2\omega_3$ (71)	ν_{NH} (13), $\omega_3 + \omega_4$ (8)
3061	$\omega_3 + \omega_4$ (79)	ν_{NH} (15)
3097	$2\omega_4$ (92)	$\omega_3 + \omega_4$ (3), ν_{NH} (1)

placements (shown in Fig. 2) at the different levels of electronic structure theory indeed reveals that in the MP2 case, two of them are somewhat more localized, i.e., they have reduced hydride bending character (namely, ω_2 and ω_3). Perhaps this is the reason for less pronounced fractionation of NH stretch character and hence of transition intensity.

The third interesting difference between the two models refers to the intensity, which is related to mode mixing, rather than to the effects of hydrogen bonding on the dipole hypersurface. As the MP2 dynamics is more localized, the intensity is distributed less uniformly. This, as well as the intrinsic strength of the NH stretching mode (see Table V), is reflected in the different band strength scales in Figs. 3 and 4.

Apart from these differences in detail between the MP2 and B3LYP models, the general pattern is uniform and fully consistent with the Fermi resonance concept. The more the NH stretching mode is scaled down, the more it picks up resonances with the ring modes. Initially, the higher frequency combination bands are activated. Later, the coupling involves also the lower ones. Beyond a certain point, which may be best represented by trace (h) in Figs. 3 and 4, the NH stretching mode starts to walk out of resonance again and the coupling amplitude decreases. The maximum width of the band pattern may be limited by the range of combination and overtone bands available in the 5D model subspace ($\approx 300\text{--}400\text{ cm}^{-1}$). However, the band width for the MP2 and B3LYP models is quite comparable to the experimental width, indicating that the major coupling partners are included.

While a rigorous labeling and reproduction of the observed transition wavenumbers and intensities is beyond the scope of the MIC model, the essential features of the resonance phenomenon and its dependence on the zeroth order frequency of the perturbed NH stretching oscillator are captured. The model makes clear how intrinsically weak combination and overtone transitions involving hydride bending amplitude light up when the NH stretching mode comes close in energy. The NH stretching character is delocalized and coherent excitation of the coupled manifold via the NH stretching transition moment leads to fast energy flow into the combined bending/ring deformation modes. Our model does not depend explicitly on the size of the pyrazole cluster, but the experimental data²¹ suggest that most of the red-shifted bands are due to trimers.

NH stretching anharmonicity

In order to further evaluate the 5D approach, a closer look at the NH stretching mode is instructive. The effective anharmonicity constant $\omega_e x_e$, 1/2 of the difference between the harmonic and the anharmonic fundamental in a local Morse oscillator approximation, may help to judge if the included degrees of freedom already reproduce a major part of the observed anharmonicity effects. Experimentally, $\omega_e x_e$ can be estimated from the fundamental²⁰ and overtone transitions of monomeric pyrazole. The latter is observed in the gas phase (0.25 cm^{-1} resolution, not shown) with its Q

TABLE IV. Effective anharmonicity constant $\omega_e x_e$ (cm^{-1}) and harmonic wavenumber ω_e (cm^{-1}) of the NH stretching vibration in pyrazole monomer, estimated by different methods, based on Morse overtone (MO) analysis of experimental (Refs. 20 and 21, and this work) and theoretical band positions, perturbation theory (PT), variational subspace treatment (5D), and Morse deuteration (MD) (Ref. 35) (see text).

$\omega_e x_e$ (cm^{-1})	ω_e (cm^{-1})	Source	Method
69	3661	Expt. ^{a-c}	MO ν_{NH} , $2\nu_{\text{NH}}$
74	3643	B3LYP	MO $\nu_{\text{NH}}^{\text{PT}}$, $2\nu_{\text{NH}}^{\text{PT}}$
70	3654	MP2	MO $\nu_{\text{NH}}^{\text{PT}}$, $2\nu_{\text{NH}}^{\text{PT}}$
86	3666	B3LYP	PT $\nu_{\text{NH}}^{\text{PT}}$, ω_{NH}
83	3680	MP2	PT $\nu_{\text{NH}}^{\text{PT}}$, ω_{NH}
68	3666	MIC B3LYP	5D $\nu_{\text{NH}}^{\text{5D}}$, ω_{NH}
65	3680	MIC MP2	5D $\nu_{\text{NH}}^{\text{5D}}$, ω_{NH}
65–159	3653–3842	Expt. ^{a,d}	MD ν_{ND} , ν_{NH}
17	3528	B3LYP	MD $\nu_{\text{ND}}^{\text{PT}}$, $\nu_{\text{NH}}^{\text{PT}}$
103	3720	MP2	MD $\nu_{\text{ND}}^{\text{PT}}$, $\nu_{\text{NH}}^{\text{PT}}$

^aReference 20.

^bReference 21.

^cThis work.

^dReference 24.

branch at 6908 cm^{-1} , whereas our current setup is not sufficiently sensitive for supersonic jet detection. From these two band centers, it follows that $\omega_e x_e^{\text{expt}} \approx 69\text{ cm}^{-1}$.

The same Morse oscillator analysis can be carried out with predictions for NH fundamental and overtone band centers based on the perturbational approach implemented in the GAUSSIAN 03 package.²⁹ The resulting parameters for the B3LYP/6–31+G* and MP2/6–311+G** levels are summarized in Table IV. There is a satisfactory agreement between the theoretical and experimental anharmonicities, considering the crudeness of the involved approximations. $\omega_e x_e$ is almost perfectly reproduced at MP2 level, whereas it is slightly too high at B3LYP level. However, the derived harmonic wavenumbers are significantly ($\approx 25\text{ cm}^{-1}$) lower than the actual values in the corresponding surfaces. This may reflect a limitation of the one dimensional (1D) Morse analysis, which would also affect the experimentally extracted ω_e and $\omega_e x_e$ values. Somewhat more likely, it reflects a deficiency of the perturbation theory implemented in GAUSSIAN 03. In any case, the perturbational B3LYP prediction of the NH stretching overtone is too low by 66 cm^{-1} or less than 1%.

To judge the 5D MIC results against the perturbation theory (PT) predictions, a 1D Morse analysis based on ω_e and the predicted anharmonic fundamental ν_{NH} is more appropriate (see Table IV). By construction, the ω_e values are the same. The anharmonicities differ significantly, the MIC predictions being in much closer agreement with the experimental value than the perturbation theory results. This may be taken as an indication that the employed perturbation theory overestimates anharmonicity and that the MIC treatment in five dimensions is remarkably accurate apart from slight deviations in the harmonic part. However, one should not dismiss the simplicity of the 1D Morse analysis. A fortuitous error compensation between the reduced coordinate space of the MIC treatment and deviations from simple

Morse oscillator behavior may also contribute. A more extended MIC treatment would be able to illuminate these deviations further.

Recently, we have used an alternative local Morse oscillator analysis based on the experimental XH (ν_{NH}) and XD (ν_{ND}) fundamentals.³⁵ If r is the ratio of the reduced ND and NH oscillator masses ($r = \mu_{\text{ND}}/\mu_{\text{NH}}$), it follows that

$$\omega_e = \frac{\nu_{\text{ND}}r - \nu_{\text{NH}}}{\sqrt{r - 1}}, \quad (7)$$

$$\omega_e x_e = \frac{\omega_e - \nu_{\text{NH}}}{2}. \quad (8)$$

This Morse deuteration approach is numerically less well conditioned than the overtone-based Morse oscillator analysis and it is more susceptible to failure due to mode mixing in the less well isolated XD stretching range. However, for hydrogen-bonded complexes, where overtone transitions are exceedingly weak, it is currently often the only experimental source for such anharmonicity estimates. In the present case, this approach suffers from a critical deficiency—Fermi resonance interaction with the $2\nu_9$ band (the fundamental of which may be found at 1315 cm^{-1}) in the monomer ND stretching mode.²⁴ For completeness, we include the resulting anharmonicity constants based on the extreme assignments of the ND stretching mode to either one of the observed bands near 2600 and 2637 cm^{-1} in Table IV. It is obvious that the resulting error bars are too large to render this analysis useful in the present case.

Harmonic calculations for substituted pyrazoles

To investigate the robustness of the Fermi resonance scenario as well as the dependence of the monomer and dimer NH stretching fundamentals on the electron density of the heterocycle, we have extended the spectroscopic studies to pyrazole homologs, in which one or two C—H groups are replaced by C—CH₃ or C—CF₃ groups. Among the investigated species, we shall discuss here the singly and doubly methylated and trifluoromethylated derivatives which are shown schematically in Fig. 5.

Their harmonic force fields were characterized at B3LYP/6-31+G* level (Table V). The NH stretching vibration is predicted to vary only weakly with methyl group substitution. Only methyl substitution in the direct neighborhood has a significant frequency lowering effect. Trifluoromethyl substitution lowers the NH stretching frequency by a larger amount, more or less independent on the substitution site and more or less additive, if two groups are introduced. At the same time, it enhances the fundamental band strength somewhat.

All substituted species show ring deformation/hydride bending vibrations in a similar range of wavenumbers (1200 – 1650 cm^{-1}), as can be seen from Table V. Ring deformation vibrations involving substituted atoms show slightly shifted frequencies corresponding to mass effects and changes in the associated XH bending character. However, the normal coordinates do not change dramatically in

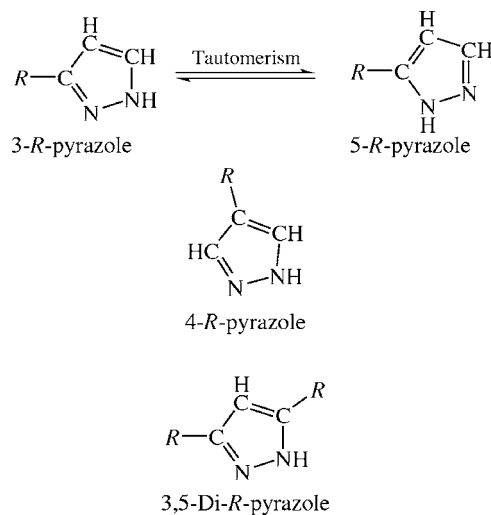


FIG. 5. Structures and tautomerism of substituted pyrazoles studied in the supersonic jet expansion. For $R \equiv \text{CH}_3$: 3(5)-methylpyrazole, 4-methylpyrazole, and 3,5-dimethylpyrazole. For $R \equiv \text{CF}_3$: 3(5)-trifluoromethylpyrazole and 3,5-bis(trifluoromethyl)pyrazole.

comparison to unsubstituted pyrazole. Therefore, one expects that the qualitative resonance pattern for the corresponding trimer NH stretching modes should persist.

Experimental results for substituted pyrazoles

Since substituted pyrazoles have a low vapor pressure, no systematic study of the stagnation pressure dependence of NH stretching spectra was attempted. This will be possible in the future using a heated nozzle assembly.²⁷ Until that is done, small dimer contributions within the larger cluster band manifold cannot be excluded. However, the close analogy of the IR spectra to those of pyrazole renders the monomer, dimer, and larger cluster assignments rather straightforward. A complication arises from the prototropic tautomerism of unsymmetric 1H-pyrazoles, as shown in Fig. 5. Only in the case of 3(5)-methylpyrazole did we observe two distinct monomer bands at 3526 and 3511 cm^{-1} . The former band is two to three times stronger. Based on the B3LYP calculations (Table V), it should be assigned to 3-methylpyrazole which is more stable by 0.6 kJ/mol . The predicted spectral splitting of 13 cm^{-1} agrees with the experimental splitting of 15 cm^{-1} . For the trifluorocompound, the two tautomers are expected to overlap based on the B3LYP prediction, which could explain why only one band is observed. Alternatively, the 4 kJ/mol energy difference (B3LYP) between the metastable five-substituted member and the more stable 3-(trifluoromethyl)pyrazole may explain why only one band is observed. Its experimental redshift of 10 cm^{-1} relative to pyrazole is reproduced by the theoretical prediction (11 – 12 cm^{-1}). The 26 cm^{-1} redshift of the bis(trifluoromethyl)pyrazole is also well reproduced at B3LYP level (25 cm^{-1}). It is certainly a consequence of the electron-withdrawing effect of the CF₃ groups. The correlation between experimental and B3LYP substitution shifts relative to pyrazole (Fig. 6) is remarkable. The good performance of the

TABLE V. Harmonic transition wavenumbers ω (in parentheses: band strengths in km mol^{-1}) of the ring stretching vibrations ω_i and the NH stretching mode ν_{NH} of the substituted pyrazoles in Fig. 5 as calculated within the B3LYP/6-31+G* approximation.

Vibration	ω (cm^{-1})
	Pyrazole
ω_1	1393 (6)
ω_2	1434 (14)
ω_3	1491 (8)
ω_4	1575 (7)
ν_{NH}	3666 (77)
	Pyrazole MP2 ^a
ω_1	1376 (3)
ω_2	1450 (11)
ω_3	1502 (7)
ω_4	1547 (5)
ν_{NH}	3680 (100)
	3-methylpyrazole/[5-methylpyrazole]
ω_1	1209 (9) [1374 (1)]
ω_2	1405 (12) [1453 (7)]
ω_3	1491 (13) [1491 (24)]
ω_4	1586 (26) [1618 (20)]
ν_{NH}	3668 (78) [3655 (62)]
	4-methylpyrazole
ω_1	1389 (4)
ω_2	1419 (8)
ω_3	1503 (1)
ω_4	1623 (2)
ν_{NH}	3667 (78)
	3,5-dimethylpyrazole
ω_1	1308 (24)
ω_2	1462 (35)
ω_3	1532 (1)
ω_4	1624 (42)
ν_{NH}	3658 (62)
	3,5-bis(trifluoromethyl)pyrazole
ω_1	1348 (97)
ω_2	1457 (37)
ω_3	1491 (0)
ω_4	1618 (27)
ν_{NH}	3641 (123)
	3-trifluoromethylpyrazole/[5-trifluoromethylpyrazole]
ω_1	1415 (31) [1339 (201)]
ω_2	1490 (13) [1468 (28)]
ω_3	1511 (52) [1498 (5)]
ω_4	1576 (1) [1614 (21)]
ν_{NH}	3654 (92) [3653 (107)]

^aMP2/6-311+G** calculation instead of B3LYP/6-31+G*.

B3LYP calculations in predicting the monomer substitution effects provides additional support for the reliability of this electronic structure approach.

A tentative dimer band assignment is indicated in Fig. 7, which collects the jet FTIR spectra in the dimer and trimer ranges. For the bis(trifluoromethyl)pyrazole, some overlap by trimer absorptions or the onset of Fermi resonance may be postulated based on the band width, whereas the other dimer bands are still rather narrow. They are characteristi-

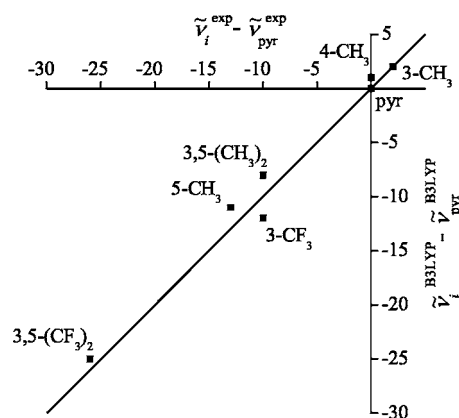


FIG. 6. Close correlation between experimental and harmonic B3LYP substitution shifts of the NH stretching bands of substituted monomeric pyrazoles $\tilde{\nu}_i$ relative to parent pyrazole $\tilde{\nu}_{\text{pyr}}$. The labels indicate the substitution pattern (see Fig. 5) and the diagonal line represents a perfect match.

cally redshifted with respect to the corresponding monomer bands. Methyl groups have a minor effect on this redshift, whereas trifluoromethyl substitution reduces it by 10% and more. Thus, the acceptor quality appears to be more influential on the hydrogen bond induced frequency shift in pyrazole dimers than the hydrogen bond donor quality, in line with earlier findings for alcohol dimers.^{27,36}

Common to all investigated pyrazoles is an extensive, structured absorption below the dimer absorption frequency (Fig. 7). It spans a range of roughly 400 cm^{-1} and can be explained in analogy to the parent compound pyrazole [trace

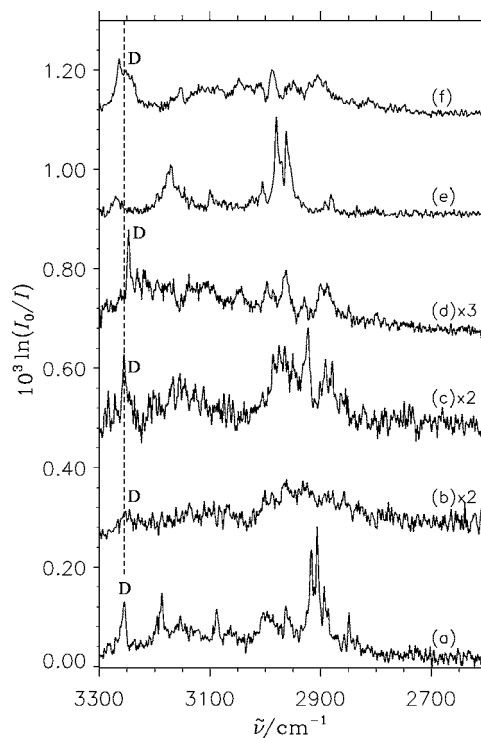


FIG. 7. FTIR jet spectra of the substituted pyrazoles. (a) pyrazole (Ref. 21), (b) 3(5)-methylpyrazole, (c) 4-methylpyrazole, (d) 3,5-dimethylpyrazole [measured with a heated nozzle assembly (Ref. 27)], (e) 3(5)-trifluoromethylpyrazole, and (f) 3,5-bis(trifluoromethyl)pyrazole. The dashed line marks the position of the dimer in the NH stretching band in the parent compound (a).

(a)]. The similarity of the spectra of pyrazole and 3(5)-(trifluoromethyl)pyrazole is particularly striking. Both are dominated by a strong doublet around 2950 cm^{-1} . However, an assignment of the detailed structure is beyond the capabilities of the MIC model. For the latter, only the coarse-grained similarity is relevant and confirms that coupling of the softened NH stretching mode to two-quantum aromatic ring excitations is quite universal for pyrazole aggregates with linear hydrogen bonds.

CONCLUSIONS AND OUTLOOK

The NH stretching mode in pyrazoles is known to exhibit a pronounced Fermi resonance pattern in condensed phases. We show by supersonic jet FTIR spectroscopy that this phenomenon is already present in small isolated clusters, presumably trimers, whereas it is largely absent in dimers of pyrazole. The resonance partners are mostly overtones and combination bands of aromatic ring vibrations with hydride bending character, which are only weakly affected by hydrogen bonding. The reason why these resonance partners only light up in trimer spectra, but not in dimers, must be sought in the energetic resonance condition itself.

By developing a monomers-in-clusters model which tunes the NH stretching vibration of monomeric pyrazole across the $3\text{--}3.5\ \mu\text{m}$ range, we can show that the essential anharmonic couplings are already laid out in the monomer. Hydrogen bonding simply serves to fulfill the energetic resonance condition by reducing the bond order of the NH chromophore. While such a model does not capture the dynamical details and long-term behavior of the energy flow out of the chromophore, it describes the primary pathway. It does so in an efficient way, as it only needs electronic structure calculations of the monomer. This allows for five dimensional variational calculations of the involved states, which would be orders of magnitude more expensive for the trimer itself.

The investigation of the anharmonicity of the NH stretching oscillator via different approaches shows that a 5D MIC calculation captures the most important coupling partners. It would be interesting to verify the present infrared coupling scenario by Raman spectroscopy.³⁷ While the MIC approach remains exactly the same, the observed symmetric NH stretching modes are predicted to be slightly further redshifted. The additional redshift is on the order of 10% and therefore, not expected to change the coupling scenario in a qualitative way. However, a combination of heated nozzle source²⁷ and improved Raman detectivity will be required to observe the totally symmetric bands.²⁵

ACKNOWLEDGMENTS

This work was supported by the Fonds der Chemischen Industrie and by the DFG research training group 782 (www.pcg.de). We thank N. Borho for help and discussions.

¹E. Fermi, *Z. Phys.* **71**, 250 (1931).

²M. Quack, *Annu. Rev. Phys. Chem.* **41**, 839 (1990).

³H. R. Dübal and M. Quack, *J. Chem. Phys.* **81**, 3779 (1984).

⁴C. Emmeluth, M. A. Suhm, and D. Luckhaus, *J. Chem. Phys.* **118**, 2242

(2003).

⁵G. M. Florio, T. S. Zwier, E. M. Myshakin, K. D. Jordan, and E. L. Sibert III, *J. Chem. Phys.* **118**, 1735 (2003).

⁶K. Heyne, N. Huse, J. Dreyer, E. T. J. Nibbering, T. Elsaesser, and S. Mukamel, *J. Chem. Phys.* **121**, 902 (2004).

⁷J. R. Dwyer, J. Dreyer, E. T. J. Nibbering, and T. Elsaesser, *Chem. Phys. Lett.* **432**, 146 (2006).

⁸J. Dreyer, *J. Chem. Phys.* **127**, 054309 (2007).

⁹C. Foces-Foces, I. Alkorta, and J. Elguero, *Acta Crystallogr., Sect. B: Struct. Sci.* **56**, 1018 (2000).

¹⁰R. Goddard, R. M. Claramunt, C. Escolástico, and J. Elguero, *New J. Chem.* **23**, 237 (1999).

¹¹L. Infantes and S. Motherwell, *Struct. Chem.* **15**, 173 (2004).

¹²J. A. Smith, B. Wehrle, F. Aguilar-Parrilla, H. H. Limbach, M. C. Foces-Foces, F. H. Cano, J. Elguero, A. Baldy, M. Pierrot, M. M. T. Khurshid, and J. B. Larcombe-McDouall, *J. Am. Chem. Soc.* **111**, 7304 (1989).

¹³F. Aguilar-Parilla, G. Scherer, H. H. Limbach, M. C. Foces-Foces, F. H. Cano, J. A. Smith, C. Toiron, and J. Elguero, *J. Am. Chem. Soc.* **114**, 9657 (1992).

¹⁴J. L. G. de Paz, J. Elguero, C. Foces-Foces, A. L. Llamas-Saiz, F. Aguilar-Parrilla, O. Klein, and H. H. Limbach, *J. Chem. Soc., Perkin Trans. 2* **1997**, 101.

¹⁵O. Klein, F. Aguilar-Parrilla, J. M. Lopez, N. Jagerovic, J. Elguero, and H. H. Limbach, *J. Am. Chem. Soc.* **126**, 11718 (2004).

¹⁶S. Schweiger and G. Rauhut, *J. Phys. Chem. A* **107**, 9668 (2003).

¹⁷D. M. W. Anderson, J. L. Duncan, and F. J. C. Rossotti, *J. Chem. Soc.* **1961**, 140.

¹⁸J. P. Castaneda, G. S. Denisov, S. Y. Kucherov, V. M. Schreiber, and A. V. Shurukhina, *J. Mol. Struct.* **660**, 25 (2003).

¹⁹W. Hückel, J. Datow, and E. Simmersbach, *Z. Phys. Chem. (Leipzig)* **186**, 129 (1940).

²⁰M. Majoube, *J. Phys. Chem.* **92**, 2407 (1988).

²¹C. A. Rice, N. Borho, and M. A. Suhm, *Z. Phys. Chem.* **219**, 379 (2005).

²²A. Zecchina, L. Cerruti, S. Coluccia, and E. Borello, *J. Chem. Soc. B* **1967**, 1363.

²³H. Wolff and H. Müller, *Spectrochim. Acta, Part A* **32**, 581 (1976).

²⁴V. Tabacik, V. Pellegrin, and H. H. Günthard, *Spectrochim. Acta, Part A* **35**, 1055 (1979).

²⁵J. M. Orza, M. V. García, I. Alkorta, and J. Elguero, *Spectrochim. Acta, Part A* **56**, 1469 (2000).

²⁶T. Häber, U. Schmitt, and M. A. Suhm, *Phys. Chem. Chem. Phys.* **1**, 5573 (1999).

²⁷C. Cézard, C. A. Rice, and M. A. Suhm, *J. Phys. Chem. A* **110**, 9839 (2006).

²⁸M. J. Frisch, G. W. Trucks, H. B. Schlegel, G. E. Scuseria, M. A. Robb, J. R. Cheeseman, J. A. Montgomery, Jr., T. Vreven, K. N. Kudin, J. C. Burant, J. M. Millam, S. S. Iyengar, J. Tomasi, V. Barone, B. Mennucci, M. Cossi, G. Scalmani, N. Rega, G. A. Petersson, H. Nakatsuji, M. Hada, M. Ehara, K. Toyota, R. Fukuda, J. Hasegawa, M. Ishida, T. Nakajima, Y. Honda, O. Kitao, H. Nakai, M. Klene, X. Li, J. E. Knox, H. P. Hratchian, J. B. Cross, C. Adamo, J. Jaramillo, R. Gomperts, R. E. Stratmann, O. Yazyev, A. J. Austin, R. Cammi, C. Pomelli, J. W. Ochterski, P. Y. Ayala, K. Morokuma, G. A. Voth, P. Salvador, J. J. Dannenberg, V. G. Zakrzewski, S. Dapprich, A. D. Daniels, M. C. Strain, O. Farkas, D. K. Malick, A. D. Rabuck, K. Raghavachari, J. B. Foresman, J. V. Ortiz, Q. Cui, A. G. Baboul, S. Clifford, J. Cioslowski, B. B. Stefanov, G. Liu, A. Liashenko, P. Piskorz, I. Komaromi, R. L. Martin, D. J. Fox, T. Keith, M. A. Al-Laham, C. Y. Peng, A. Nanayakkara, M. Challacombe, P. M. W. Gill, B. Johnson, W. Chen, M. W. Wong, C. Gonzalez, and J. A. Pople, GAUSSIAN03, Revision B.04, Gaussian, Inc., Wallingford, CT, 2004.

²⁹V. Barone, *J. Chem. Phys.* **122**, 014108 (2005).

³⁰A. Beil, D. Luckhaus, R. Marquardt, and M. Quack, *Faraday Discuss.* **99**, 49 (1994).

³¹D. Luckhaus, M. J. Coffey, M. D. Fritz, and F. F. Crim, *J. Chem. Phys.* **104**, 3472 (1996).

³²D. Luckhaus, *Ber. Bunsenges. Phys. Chem.* **101**, 346 (1997).

³³D. Luckhaus, *J. Chem. Phys.* **106**, 8409 (1997).

³⁴D. Luckhaus, *J. Chem. Phys.* **113**, 1329 (2000).

³⁵R. W. Larsen, P. Zielke, and M. A. Suhm, *J. Chem. Phys.* **126**, 194307 (2007).

³⁶H. Schaal, T. Häber, and M. A. Suhm, *J. Phys. Chem. A* **104**, 265 (2000).

³⁷P. Zielke and M. A. Suhm, *Phys. Chem. Chem. Phys.* **8**, 2826 (2006).